

# X-ray structure of a voltage-dependent K<sup>+</sup> channel

Youxing Jiang\*, Alice Lee, Jiayun Chen, Vanessa Ruta, Martine Cadene, Brian T. Chait & Roderick MacKinnon

Howard Hughes Medical Institute, Laboratory of Molecular Neurobiology and Biophysics, Laboratory of Mass Spectrometry and Gaseous Ion Chemistry, Rockefeller University, 1230 York Avenue, New York, New York 10021, USA

**Voltage-dependent K<sup>+</sup> channels are members of the family of voltage-dependent cation (K<sup>+</sup>, Na<sup>+</sup> and Ca<sup>2+</sup>) channels that open and allow ion conduction in response to changes in cell membrane voltage. This form of gating underlies the generation of nerve and muscle action potentials, among other processes. Here we present the structure of KvAP, a voltage-dependent K<sup>+</sup> channel from *Aeropyrum pernix*. We have determined a crystal structure of the full-length channel at a resolution of 3.2 Å, and of the isolated voltage-sensor domain at 1.9 Å, both in complex with monoclonal Fab fragments. The channel contains a central ion-conduction pore surrounded by voltage sensors, which form what we call ‘voltage-sensor paddles’—hydrophobic, cationic, helix-turn-helix structures on the channel’s outer perimeter. Flexible hinges suggest that the voltage-sensor paddles move in response to membrane voltage changes, carrying their positive charge across the membrane.**

Many cells produce electrical impulses, known as action potentials, that propagate along their surface membrane. Action potentials travel quickly, and their arrival at a distant location initiates cellular processes such as the release of neurotransmitter molecules or the contraction of muscles<sup>1</sup>. These electrical impulses are the means by which living cells transfer information over large distances in short time intervals, allowing information processing in the nervous system, movement and many other processes.

Fifty years ago, Hodgkin and Huxley presented the theory of the action potential, which included two key elements—that the membrane of a cell can undergo transient changes in its selective permeability to Na<sup>+</sup> and K<sup>+</sup> ions, and that the permeability changes depend on membrane voltage<sup>2</sup>. These two elements create an interesting situation, because selective permeability to ions determines the membrane voltage, and the voltage determines the permeability. The feedback relationship between membrane voltage and ion permeability, combined with the ‘electrical cable’ properties of a cylindrical membrane, gave an accurate description of action potentials in squid giant axons.

These key elements of the Hodgkin–Huxley theory are embodied in a single family of protein molecules known as the voltage-dependent cation channels<sup>1</sup>. This family includes K<sup>+</sup>-, Na<sup>+</sup>- and Ca<sup>2+</sup>-selective members. When the pore of a voltage-dependent cation channel opens, it selectively conducts predominantly its namesake ion. The control of pore opening—the process known as gating—is dependent on the membrane voltage, hence the name ‘voltage-dependent channel’.

How does a voltage-dependent channel ‘sense’ the membrane voltage and gate open as a function of its value? It is thought that charged amino acids called ‘gating charges’ move through the membrane electric field in association with pore opening, allowing membrane voltage to bias the equilibrium between closed and opened conformations<sup>3–5</sup>. Gating charge movements can be measured as transient electrical currents associated with gating, separate from ion conduction<sup>3</sup>. In K<sup>+</sup> channels, the gating charge per tetrameric channel corresponds to 12–14 electron charges (3.0–3.5 charges per subunit) crossing the entire membrane voltage difference<sup>6–8</sup>. This large gating charge gives rise to a steep change in open probability as a function of membrane voltage.

All members of the voltage-dependent cation channel family

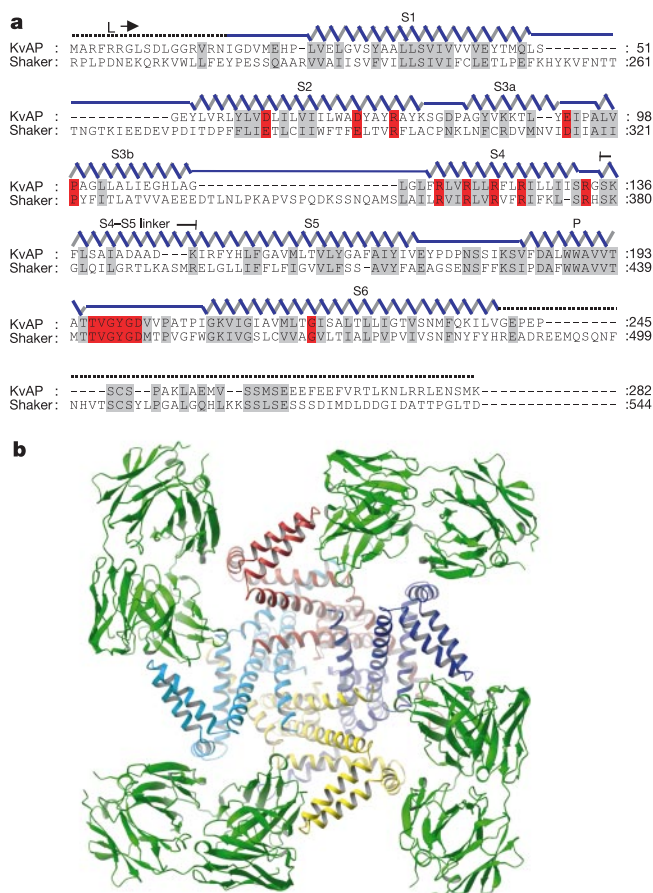


**Figure 1** Structure of the KvAP channel. **a**, Sequence alignment of KvAP and the Shaker K<sup>+</sup> channel. Regions of high homology are coloured grey, and residues known to be important for K<sup>+</sup> selectivity and voltage-dependent gating are coloured red. Secondary structure elements show S1–S6 and P (pore)  $\alpha$ -helices on the basis of the crystal structure. Disordered regions are shown as black dotted lines. The first five residues of KvAP were replaced by a single leucine (L) during expression. **b**, Structure of the KvAP channel (blue, yellow, cyan and red helical structures) bound to four Fab fragments (green), viewed down the four-fold axis from the intracellular side. This and all subsequent ribbon diagrams were generated with the program RIBBONS<sup>42</sup>.

\* Present address: University of Texas Southwestern Medical Center, Department of Physiology, 5323 Harry Hines Blvd, Dallas, Texas 75390-9040, USA.

contain six hydrophobic segments per subunit, S1–S6 (refs 9–11). Four subunits (most often identical in K<sup>+</sup> channels, and linked together as homologous ‘domains’ in Na<sup>+</sup> and Ca<sup>2+</sup> channels) surround a central ion-conduction pore. S5–S6 line the pore and determine ion selectivity, whereas S1–S4 form the voltage sensors. Certain charged amino acids within the voltage sensors, particularly the first four arginines in S4, account for most of the gating charge<sup>7,8</sup>. Studies with thiol-reactive compounds<sup>12–15</sup> and fluorescently labelled channels<sup>5,16,17</sup> have documented conformational

changes in the region of S4 during gating, and form the basis of the prevailing model, in which S4 helices move along a path surrounded by protein, shielded from lipid<sup>18–20</sup>.

We have studied the mechanism of voltage-dependent gating using biochemical, X-ray crystallographic and electrophysiological methods. Our studies focus on a voltage-dependent K<sup>+</sup> channel, KvAP, from the thermophilic archaebacteria *Aeropyrum pernix*. This channel is closely related in amino-acid sequence to, and exhibits all of the electrophysiological properties of, eukaryotic Kv

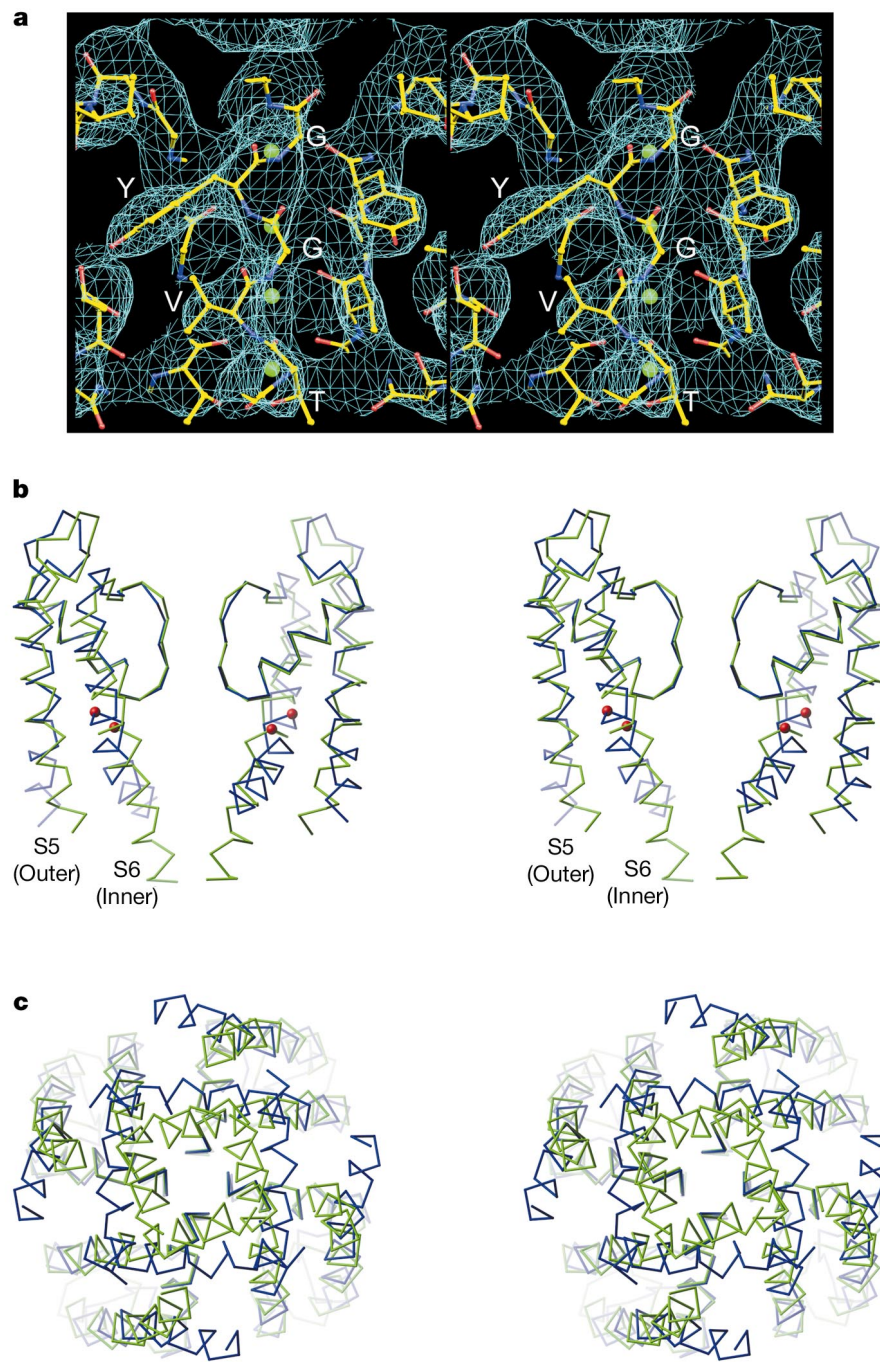


**Figure 2** Stereo view of the KvAP pore and comparison with the KcsA K<sup>+</sup> channel. **a**, An electron density map at 1.0  $\sigma$  contour (blue mesh) was calculated from the Fab model used in molecular replacement after rigid-body refinement. The refined model of the selectivity filter is shown with carbon, nitrogen and oxygen atoms coloured yellow, blue and red, respectively. The positions of four K<sup>+</sup> ions are shown as green spheres.

The  $\alpha$ -carbon traces of the KvAP pore (blue) and the KcsA K<sup>+</sup> channel (green) are shown from the side in **b** and from the intracellular solution in **c**. Outer and inner helices are labelled S5 and S6, respectively. The glycine-gating hinges are shown as red spheres.

Table 1 Data and refinement statistics

Protein	Fab 6E1-KvAP	Fab 33H1-isolated voltage sensor
Space group	I422	C2
Data source*	CHESS A1	CHESS A1
Resolution (Å)	30–3.2	30–1.9
Completeness (%)	98.8 (95.2)	97.1 (92.8)
Redundancy†	5.5	2.9
$R_{\text{sym}} (\%) \ddagger$	8.0 (42.4)	5.8 (17.7)
$\text{I}/\sigma$	18 (2.2)	15.5 (5.8)
Unique reflections	22,476	56,778
Atoms refined	5,046 protein, 6 H <sub>2</sub> O, 6 K, 7 Cd	4,365 protein, 403 H <sub>2</sub> O
$R_{\text{work}}/R_{\text{free}} (\%) \S$	25.6/29.9	23.1/25.1
r.m.s.d. of bond	1.44°/0.009 Å	1.48°/0.006 Å

\* Data listed are those used for refinement. Numerous data sets were also collected at CHESS F1 and NSLS X25.

† Redundancy represents the ratio of the total number of measurements to the number of unique reflections.

‡  $R_{\text{sym}} = \sum |I_i - \langle |I_j| \rangle| / \sum |I_i|$ , where  $\langle |I_j| \rangle$  is the average intensity of symmetry-equivalent reflections.

§ R factor =  $\sum |F(\text{obs}) - F(\text{calc})| / \sum |F(\text{obs})|$ ; 5% of the data that were excluded from refinement were used in the  $R_{\text{free}}$  calculation.

|| r.m.s.d. of bond is the root-mean-square deviation of bond angle and length.

Numbers in parentheses are statistics for last resolution shell.

channels<sup>21</sup>. We describe the structure of KvAP and two conformations of its voltage sensor. The structure of the voltage sensor is very unexpected. In a companion paper<sup>22</sup>, we test mechanistic predictions of this structure to begin to understand how the channel senses membrane voltage to open its pore.

### Structure determination

We examined many different bacterial K<sup>+</sup> channels that contain amino-acid sequences corresponding to the voltage sensor. For six of these channels, we succeeded in expressing milligram quantities

of tetrameric channels, but in every case they aggregated into multiples of tetramers during concentration, and never crystallized. Even after reconstitution into lipid membranes at high protein-to-lipid ratios, rafts of closely packed channels did not form ordered arrays, which suggested that the voltage sensor might be a very mobile structure, making crystallization difficult. With this difficulty in mind, we initiated a search for voltage-dependent K<sup>+</sup> channels in extreme thermophiles, hoping to identify an exceptionally stable family member.

Figure 1a shows the sequence of KvAP from *Aeropyrum pernix*<sup>21</sup>, together with the *Shaker* K<sup>+</sup> channel sequence<sup>11</sup>. Amino acids that are known to be crucial for ion selectivity and voltage-dependent gating are highlighted in red to emphasize the relatedness of these two voltage-dependent K<sup>+</sup> channels. KvAP was expressed and purified, and remained as a mono-dispersed tetramer in a variety of detergents. During expression in *Escherichia coli*, we found it necessary to block K<sup>+</sup> channels with 10 mM BaCl<sub>2</sub> to reduce toxicity to bacteria and to obtain properly folded protein<sup>21</sup>. For an unknown reason, the expressed KvAP channel contains a leucine in place of the first five amino acids encoded by the KvAP gene (see Methods).

Even the KvAP channel failed to crystallize under a wide range of conditions. To overcome the potential flexibility of the voltage-sensor regions, we reasoned that if we could ‘hold’ the channel with a Fab fragment attached to each of its four voltage sensors, we might favour crystallization. To this end, we raised monoclonal antibodies against the channel, and selected those that could bind to the voltage sensor (see Methods). These were produced in large quantity, and used (as Fab fragments) in crystallization trials. One of these (Fab 6E1) yielded crystals that diffracted X-rays to 3.2-Å Bragg spacings

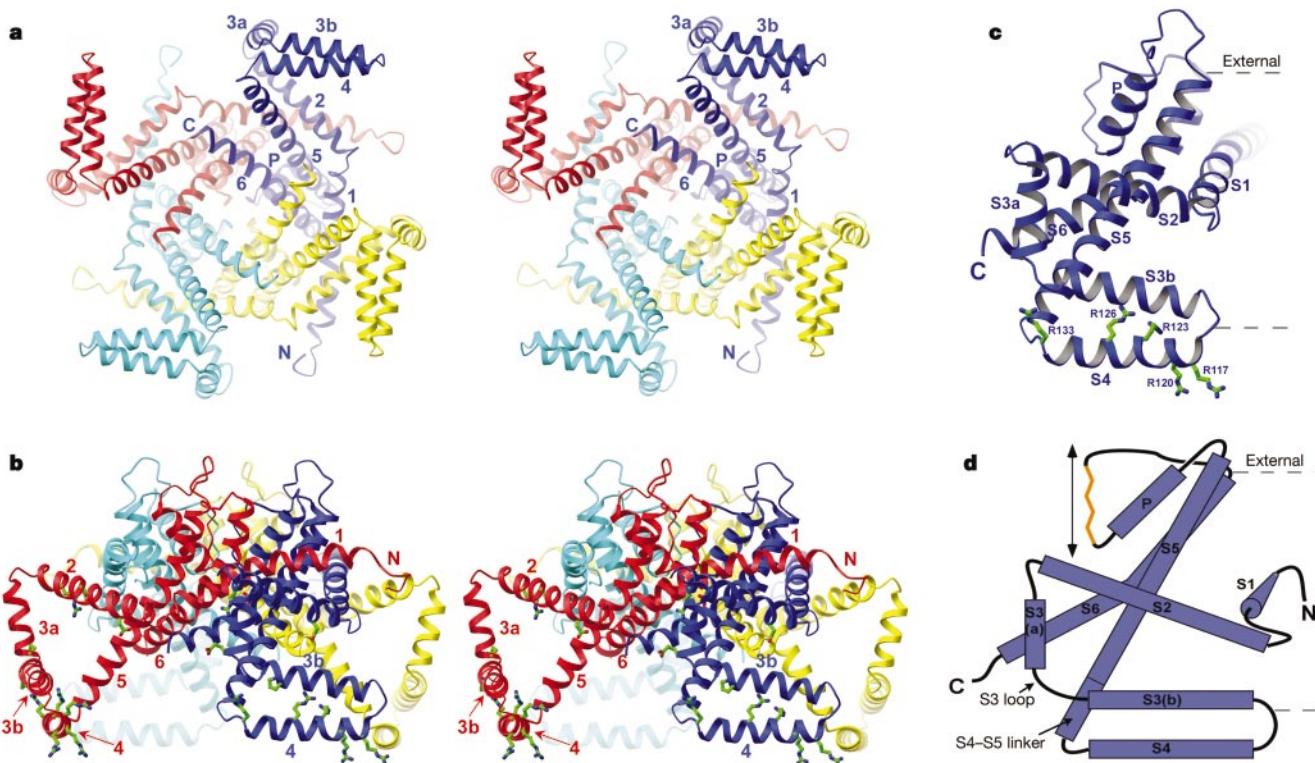


**Figure 3** Architecture of the KvAP channel. **a**, Stereo image of the KvAP channel tetramer viewed from the intracellular side of the membrane. Each subunit is a different colour; helical elements of the blue subunit are labelled numerically for S1–S6 and with P for the pore helix. N and C mark the termini. **b**, Stereo image of the KvAP channel tetramer viewed from the side with the intracellular solution below. Views in **a** and **b** are related by a 90° rotation about a horizontal axis. Side chains of selected residues known to be involved

in voltage-dependent gating are shown on the blue and red subunits. Selected helical elements are labelled on the red and blue subunits. **c**, A single KvAP subunit viewed from the same perspective as in **b**. Conserved arginine residues on the voltage-sensor paddle are shown. **d**, A schematic diagram of the KvAP subunit topology is shown with an orange selectivity filter and an arrow to indicate the ion pathway. The demarcation between the S4–S5 linker and S5 is indicated by a black line.

at the synchrotron. Phases were determined by molecular replacement using a Fab search model, and after rigid-body refinement, they yielded a map with interpretable electron density in the channel region (Fig. 2a). Difference Fourier maps calculated with Hg derivative data from site-directed cysteine mutants were used to guide model building (see Methods). A complete model from amino acid 18 to 240 including all side chains was refined to a free residual of 29.9% (Table 1). The crystallographic solution reveals a four-fold symmetric tetramer with a Fab bound at the outer perimeter of each subunit (Fig. 1b).

### The ion-conduction pore

Because of its high conservation among K<sup>+</sup> channels, the selectivity filter (sequence TVGYG) was the one region of the KvAP channel where we could predict what the structure ought to look like. As expected, the filter is essentially identical to that in KcsA<sup>23,24</sup> (Fig. 2a). The filter features carbonyl oxygen atoms directed towards the pore to coordinate dehydrated K<sup>+</sup> ions, and hydrophobic side chains of valine and tyrosine directed into a hydrophobic core surrounding the filter to stabilize the main chain. Although certain amino-acid side chains within the hydrophobic core surrounding the filter are different from those found in KcsA, a comparison of  $\alpha$ -carbon traces shows almost perfect superposition (Fig. 2b). The near invariance of the selectivity filter structure in the context of channels (KcsA and KvAP) with very different gating mechanisms is not surprising, because in both channels the filter serves the same function, to conduct K<sup>+</sup> ions rapidly and selectively.

The structures of the KvAP and KcsA pores deviate within the region of the intracellular membrane leaflet (Fig. 2b, lower half).

The S6 helices (also known as inner helices<sup>23</sup>), which line the ion pathway below the selectivity filter, begin to diverge most noticeably at a point referred to as the glycine-gating hinge (Fig. 2b, red spheres). The gating hinge was identified when comparing the structures of KcsA (a closed K<sup>+</sup> channel) and MthK (an opened K<sup>+</sup> channel), and observing that the inner helices seem to open like the aperture of a camera by bending at a glycine residue<sup>25</sup>. This glycine is conserved at a specific location in the inner helix of many K<sup>+</sup> channels, including KvAP, and has been proposed to underlie gating<sup>26</sup>. Bending of the inner helix at the glycine-gating hinge position of KvAP suggests that it may gate open by similar movements.

The KvAP channel is opened wider than the closed KcsA K<sup>+</sup> channel<sup>23</sup> (Fig. 2c)—nearly as wide as the opened MthK channel<sup>25</sup>. We think that the KvAP channel has an opened pore because of crystal packing interactions, which pull the outer helices away from the pore axis; we will return to this point later when considering the mechanism by which the voltage sensor may exert force on the pore to open it. For now, we wish to highlight one important feature of the structural comparison in Fig. 2c: in both KvAP and KcsA, the adjacent inner (S6) and outer (S5) helices of each subunit maintain an approximately antiparallel relationship to one another. That is, the inner and outer helices seem to move together as a single unit. This observation raises the interesting possibility that the voltage sensor, which is attached directly to the outer helix, might open the pore by pulling the outer helices away from the central pore axis, causing the inner helices to follow.

### The voltage sensors

The S1–S4 helices are attached to the pore as shown in Fig. 3a–c. A view down the four-fold axis from inside the cell shows that the S6 and S5 helices from each subunit encircle the ion pathway, as would be expected from the KcsA<sup>23</sup> and MthK<sup>25</sup> structures. Unexpectedly, however, S1 and S2 form the next concentric layer of helices outside S5, and S3 and S4 are located at the channel's outer perimeter (Fig. 3a). The voltage sensor has been described in the past as a set of four helical segments, on the basis of amino-acid sequence analysis. The structure shows that the traditional notation needs to be revised, as shown in Fig. 3. Contained within the traditional definition of the S3 helix there are two individual helices (S3a and S3b) separated by a loop (S3 loop). The second helix in S3, S3b, and the amino-terminal half of the traditionally defined S4 are packed tightly against each other, forming a helix-turn-helix structure that is mainly hydrophobic, with the notable exception of distributed arginine residues (Fig. 3b, c, green). We call this S3b–S4 unit the voltage-sensor paddle. The arginine residues on the paddle are highly conserved among voltage-dependent K<sup>+</sup> channels<sup>4,5</sup>, and the first four have been shown to account for most of the gating charge movement that underlies opening and closing of the pore<sup>7,8</sup>. The Fab 6E1 is bound at the tip of each paddle, to the turn connecting S3b to S4 (Fig. 1b).

Several aspects of this structure are unexpected, but a second structure (below) will help to explain why by showing that the voltage sensor is intrinsically flexible, and is capable of adopting more than one conformation. The most unexpected finding is the position of the S4 helices, which are near the intracellular membrane surface, perpendicular to the pore axis (Fig. 3). This finding apparently contradicts solid electrophysiological data showing that toxins and thiol-reactive compounds can react with the N-terminal portion of S4 from the extracellular side of the membrane, but never from the intracellular side<sup>13–15,27</sup>. How can this position of S4 helices in the crystal structure be reconciled with the electrophysiological studies? The structure shows that the voltage-sensor paddles are flanked on their N-terminal limit by the S3 loop, and on their carboxy-terminal limit by a sharp turn at a glycine residue into S5, the first several turns of which correspond to the C-terminal portion of the traditionally defined S4, referred to here as the S4–S5 linker

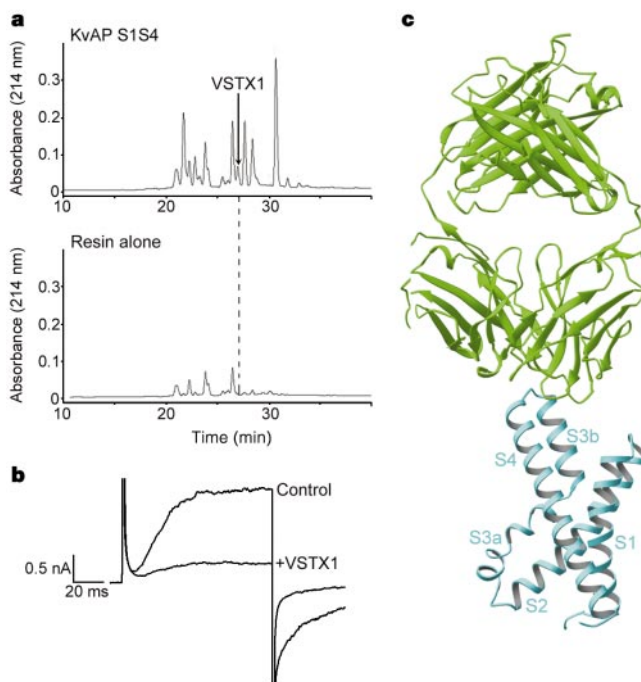


**Figure 4** Functional and structural analysis of the isolated voltage-sensor domain. **a**, The isolated voltage sensor retains its ability to bind tarantula toxins that specifically inhibit voltage sensors. A voltage-sensor affinity column was constructed by saturating Co<sup>2+</sup> affinity resin with the voltage-sensor protein. The column retained toxin components (top), including the known active VSTX1 (arrow), whereas a column formed from the Co<sup>2+</sup> resin alone did not (bottom). Graphs show reverse-phase HPLC chromatograms of toxins eluted from the Co<sup>2+</sup> columns. **b**, VSTX1 inhibits KvAP channel currents elicited by a +100 mV depolarization. **c**, Structure of the isolated voltage sensor (cyan) bound to Fab 33H1 (green).

(Fig. 3c, d). These connections should allow the voltage-sensor paddles to move rather freely with respect to the main body of the channel inside the membrane, and possibly account for the above-mentioned difficulty in crystallization. Could it be that the voltage-sensor paddles' loose attachment to the pore allowed the Fabs to extend the hinges and pull the paddles towards the cytoplasm to accommodate packing in the crystal? To address this question, we carried out further experiments.

We expressed a partial channel corresponding to S1–S4 (the isolated voltage sensor) in the absence of the ion-conduction pore. This is an unusual approach—to produce only part of an integral membrane protein—but the outcome is informative. The isolated voltage sensor is a monomer on gel filtration—not surprisingly, because the subunits of a K<sup>+</sup> channel tetramerize through the pore-forming S5, P (pore) and S6 helices, with S1–S4 located out on the perimeter (Fig. 3). We examined whether the isolated voltage sensor retains a native structure by asking whether it can recognize and bind to protein toxins that specifically inhibit voltage-sensor movements<sup>27,28</sup>. By attaching the isolated voltage sensor to resin on a column, we found that it efficiently purifies toxins from tarantula venom (Fig. 4a), and that these toxins inhibit functional KvAP channels in an electrophysiological assay (Fig. 4b). Some of the toxins we have identified in this way are the same as those previously described, such as VSTX1 (ref. 21), whereas others are new members of the family of voltage-sensor toxins. For our immediate purpose, however, this assay indicates that the isolated voltage sensor retains native structure, otherwise it would not exhibit molecular specificity for protein toxins that have evolved to bind to the voltage sensor with high affinity.

We determined the structure of the isolated voltage sensor in a complex with a Fab at 1.9-Å resolution by X-ray crystallography (Table 1 and Fig. 4c). In this isolated domain structure, the voltage

sensor is not constrained by its attachment to the pore. We again solved the phase problem by molecular replacement using a Fab search model, and refined a complete atomic model to a free residual of 25.1%. The Fab (33H1) was raised against the full-length channel and selected on the basis of its binding to the voltage sensor (somewhere within S1–S4), as described in the Methods. We note that Fab 33H1 (in the isolated voltage-sensor structure) and Fab 6E1 (in the full-length channel structure) bind to precisely the same epitope, with the same relative orientation, at the tip of the voltage-sensor paddle (Figs 1b and 4c).

Figure 5a shows the structure of the isolated voltage sensor. It contains an arrangement of helices S1, S2, S3a, S3b and S4. An S3 loop between S3a and S3b, and a voltage-sensor paddle formed by S3b and the N-terminal half of S4, are immediately recognizable. Side-chain structures of highly conserved and functionally important voltage-sensor amino acids, highlighted red in the alignment in Fig. 1a, are well defined at 1.9-Å resolution and are shown in detail (Fig. 5a). The first four arginine residues (positions 117, 120, 123 and 126) on the voltage-sensor paddle are exposed to solvent in the crystal. These are the ones shown to carry most of the gating charge in the *Shaker* K<sup>+</sup> channel<sup>7,8</sup>. The fifth S4 arginine (position 133) makes a salt bridge with aspartate 62, appearing to glue S4 and S2 together right beside the S3 loop. We note that arginine 133 in KvAP aligns most closely with arginine 377 in the *Shaker* K<sup>+</sup> channel S4 (Fig. 1a), and that *Shaker* K<sup>+</sup> channel function is destroyed when this residue is mutated<sup>5</sup>. A salt-bridge network involving arginine 76 in S2, aspartate 72 one helix turn away in S2, and glutamate 93 in S3a, seems to bridge S3a to the C-terminal half of S2. Lysine 136 in KvAP, which is conserved in the *Shaker* K<sup>+</sup> channel as lysine 380 (Fig. 1a) but not in all voltage-dependent K<sup>+</sup> channels, also participates in this salt-bridge network. The overall distribution of basic and acidic amino acids in the isolated voltage-sensor

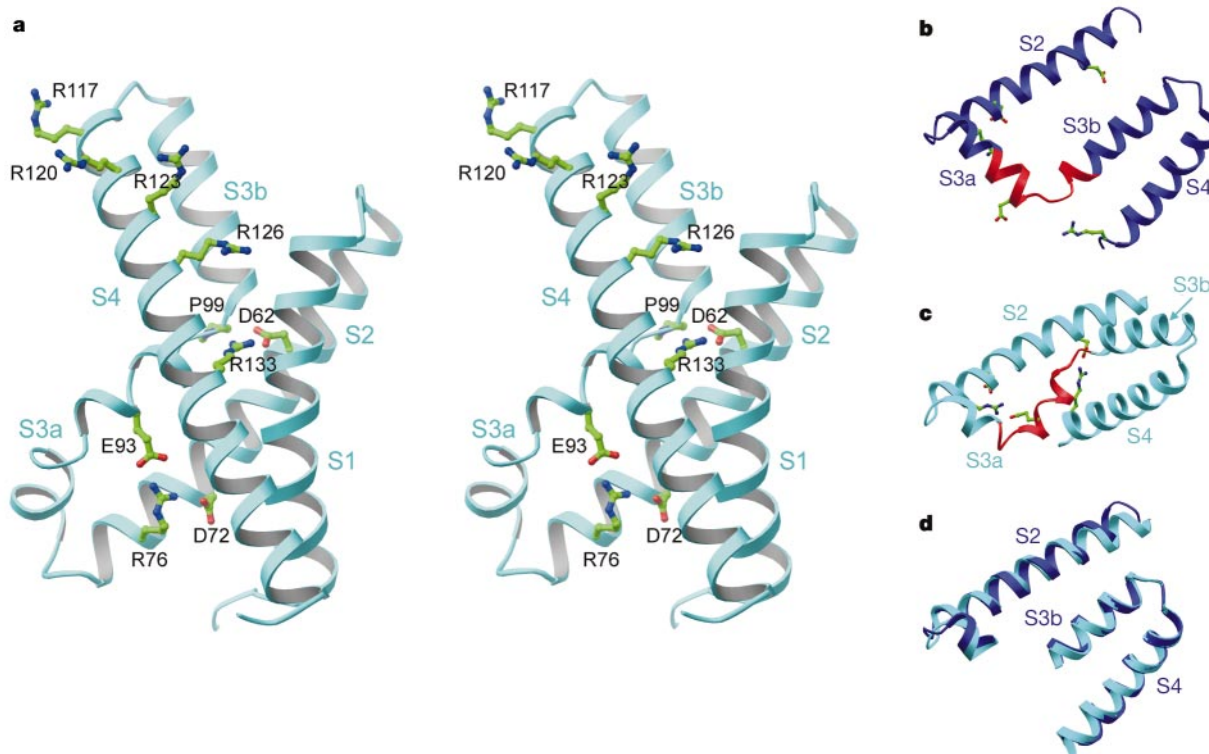


**Figure 5** Structure of the isolated voltage sensor. **a**, Stereo view with helical elements labelled in cyan and selected amino acids labelled in black using the single-letter code. **b–d**, The voltage sensor from the beginning of S2 to the end of the voltage-sensor paddle is shown for the full-length KvAP channel (**b**), for the isolated voltage sensor (**c**),

and with S2 and the voltage-sensor paddle from both structures superimposed (**d**). Amino acids forming salt bridges in the isolated voltage sensor are shown, and the S3 loop is coloured red.

structure, and the involvement of specific pairs in salt-bridge formation, explains why these residues are so highly conserved among voltage-dependent K<sup>+</sup> channels.

In Fig. 5b-d, we compare the voltage-sensor structures from the full-length channel (blue) and the isolated domain (cyan). Two regions are essentially identical, the S2 helix including the turn into S3, and the voltage-sensor paddle (Fig. 5d). However, the relative positions of these regions are different in the two structures: in the full-length channel (Fig. 5b), they are more separated and the salt bridges are broken. This conformational difference is allowed because of the flexible S3 loop that connects S2 to the voltage-sensor paddle through S3a (Fig. 5b, c, red). The significance of this S3 loop to the positions of the voltage-sensor paddles in the full-length channel crystal structure (Fig. 3), and to the dynamic properties of the voltage-sensor paddles in the membrane, will become apparent<sup>22</sup>.

There are two major differences between the voltage sensor in the full-length structure and the isolated domain: first, S1 is folded back in the isolated domain (Fig. 5a; see below); and second, S4 is straight in the isolated domain (Fig. 5a) and bent in the full channel (Fig. 3), the bend occurring just after the voltage-sensor paddle. The reason for the S4 difference is clear: in the full-length channel, S4 bends at a glycine residue to redirect the helix into S5, whereas in the isolated voltage sensor, S4 is unrestrained and continues as a straight helix. It is significant that the amino-acid sequence corresponding to the N-terminal half of the traditionally defined S4, which forms the paddle and is structurally identical in both the full-length and

isolated voltage sensors, is conserved (Fig. 6a, b), whereas the sequence of the C-terminal half, labelled 'S4–S5 linker' in Fig. 6b, is poorly conserved, contains many hydrophilic amino acids, and tends to be sprinkled with glycine residues. These sequence characteristics (Fig. 6b) and structural comparisons (Figs 3 and 5) lead us to conclude that the voltage-sensor paddle is a conserved structural unit in voltage-dependent K<sup>+</sup> channels, but that the S4–S5 linker is a helix with break points that bend easily when force is applied. Where the bends occur and their exact angles may depend on the relative positions of the voltage-sensor paddles and pore; that is, on the gating state of the channel. The hydrophilic character of the S4–S5 linker suggests that it is well suited to be at the interface with water on the intracellular side of the membrane.

The isolated voltage sensor provides insight into why S4 is in an unexpected position, projecting beyond the cytoplasmic interface in the full-length channel crystal structure (Fig. 3). The full-length channel (Fig. 7a) is compared to the pore with the isolated voltage sensor (from the beginning of S2 to the end of the voltage-sensor paddle) docked onto it (Fig. 7b); docking was accomplished by placing S2 of the isolated voltage sensor into the location of S2 in the full-length channel. The comparison gives the immediate impression that the Fabs simply pulled the paddles down by extending their attachment through the S3 loop. The remaining gap between the voltage-sensor paddle and S5 could easily be accommodated by introducing a bend into the S4–S5 linker, which corresponds to three-and-a-half helical turns at the bottom of S5 (Fig. 7). This comparison leads us to conclude that the full-

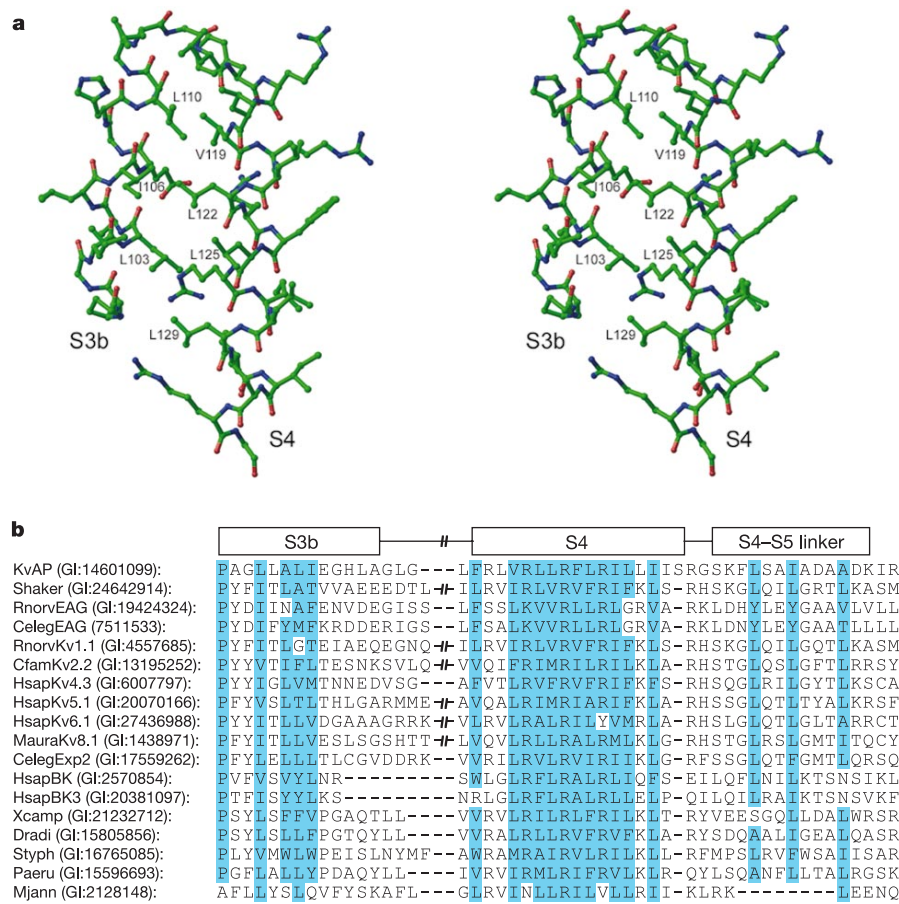


**Figure 6** The voltage-sensor paddle is conserved. **a**, Stereo view of the voltage-sensor paddle. Hydrophobic residues forming the tightly packed interface between S3b and S4 are labelled. **b**, A multiple sequence alignment of a portion of the voltage sensor from a variety of voltage-dependent K<sup>+</sup> channels shows strong conservation of residues (cyan) in

the region corresponding to the paddle, and weaker conservation in the S4–S5 linker. Alignment was generated using ClustalW<sup>43</sup> followed by manual adjustment and exclusion of loops between S3b and S4 as indicated by slashes.

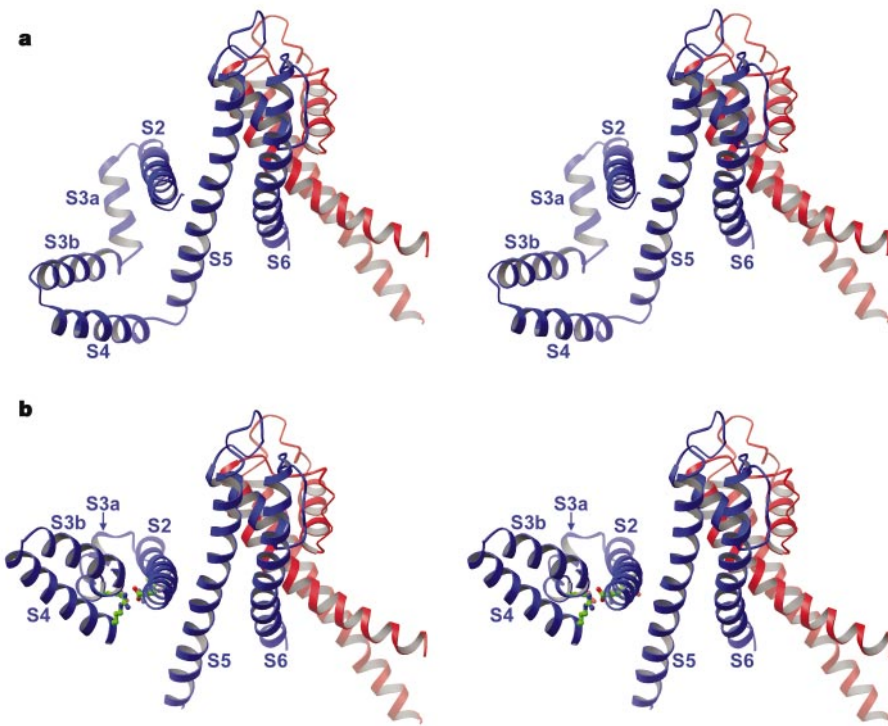


**Figure 7** Effect of Fabs on voltage-sensor conformation. **a**, Stereo view of two subunits (blue and red) from the full-length channel viewed from the side with the intracellular solution below. **b**, Identical view of the pore (S5–S6) with the isolated voltage sensor

docked according to the position of S2 in the full-length channel. The Asp 62–Arg 133 salt bridge is shown.

length channel crystal structure is actually not very far from a membrane-bound conformation. In the accompanying paper, we provide further evidence for this conclusion by determining the positions of the paddles within the lipid membrane<sup>22</sup>.

Beyond the insight into how the Fabs have altered the voltage

sensors, comparison of two voltage-sensor structures offers information about their function. The voltage sensors would not so easily have conformed to crystal packing forces imposed by the Fabs if they did not contain a high degree of natural flexibility. Not only are the voltage-sensor paddles flexibly attached to S2 and S5, but S2 and S1 are loosely packed against the pore (Figs 3 and 7a). The entire voltage sensor would appear to float inside the membrane like a separate, mobile domain. Experiments by Lu and co-workers<sup>29</sup>, who produced functional voltage-dependent K<sup>+</sup> channels by splicing the *Shaker* K<sup>+</sup> channel voltage sensor onto the KcsA pore (which does not interact naturally with a voltage sensor), support the same conclusion of loosely attached voltage-sensor domains; their chimaera channel would probably not function if the voltage sensors had to form a tight-fitting complementary interface with the pore.

In the *Shaker* K<sup>+</sup> channel, glycosylation studies<sup>30</sup> and tethered blockers<sup>31</sup> place the loop between S1 and S2 (which is larger than in KvAP by 19 amino acids; Fig. 1a) near the extracellular solution. The position of this loop in the middle of the membrane in KvAP could be a manifestation of the loose packing of S1 and S2 against the pore: we do not know to what extent the positions of these helices in the crystal deviate from that in the membrane, nor to what extent they move with gating. Furthermore, whether in the membrane S1 overlies an adjacent voltage sensor (as in the full-length channel; Fig. 3) or folds back (as in the isolated voltage sensor; Fig. 5) is unknown; a folded-back conformation would cause S1 to run straight into the cytoplasm. Despite these uncertainties, which are related to the voltage sensors' intrinsic flexibility, we know that S1 and S2 are against the pore and that the voltage-sensor paddles are at the protein–lipid interface.

The degree to which a protein's structure can be altered by crystal lattice forces depends on how rigid the protein is, and rigidity is related to function. This point can probably be best appreciated by

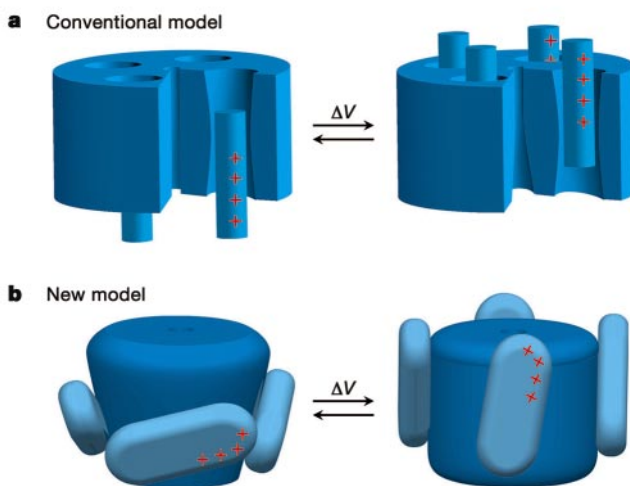


**Figure 8** Hypothesis for gating charge movements. **a**, The conventional model of voltage-dependent gating posits that the gating charges are carried through the protein core by translations and/or rotations of S4 helices, which move independently of other protein segments within a 'gating pore' or 'canaliculus'. **b**, In the new model, gating charges (red plus signs) could be carried through the membrane from inside (bottom) to outside (top) by movements of the voltage-sensor paddles against the lipid membrane, which in turn could open the pore.

examining the different regions of the KvAP channel itself. Near the selectivity filter, the pore is rigid, otherwise it would be difficult to explain the near-perfect superposition of KvAP and KcsA (Fig. 2b)—different K<sup>+</sup> channels in different crystals. The filter's rigidity makes sense in terms of its function, because it needs to be structurally constrained to discriminate between ions on the basis of small size differences. The voltage sensor (and cytoplasmic portions of the inner and outer pore-lining helices that gate the pore), by comparison, is flexible—capable of assuming different conformations (Fig. 5b–d). This property is related to its function as a voltage sensor: to sense voltage differences and open the pore, the voltage sensor has to move and rearrange itself within the membrane.

## Summary

The KvAP voltage-dependent K<sup>+</sup> channel contains a canonical K<sup>+</sup> pore surrounded by voltage sensors. The voltage sensors feature S1 and S2 helices beside the pore, and voltage-sensor paddles on the outer perimeter. The voltage-sensor paddles are helix-turn-helix structures made from S3b and the N-terminal half of S4. Their amino-acid composition is mainly hydrophobic, with the important exception of S4 arginine residues. The paddles are movable with respect to the pore because of their flexible attachment via S3 loops. Movements of the paddles would be coupled to movements of S5 helices, and hence the pore, through the S4–S5 linker.

This structure has clear implications for how the voltage-sensor paddles might move in response to changes in the membrane voltage, and open the pore. In the crystal structure, the voltage-sensor paddles are located near the intracellular side of the channel, but electrophysiological studies using spider toxins and thiol-reactive compounds have shown that amino acids on the paddle can become exposed to the extracellular solution<sup>13–15,27</sup>. These observations lead us to propose that the voltage-sensor paddles move across the membrane, carrying their cargo of gating charges through the electric field. Conventional models of voltage-dependent gating have posited that S4 helices move within their own protein-lined pathways, shielded from the lipid membrane by other parts of the protein (for example, S1, S2 and S3)<sup>18–20</sup>, as depicted in Fig. 8a. Our results now lead us to a dramatically different picture, depicted in Fig. 8b. This new picture reminds us of Finkelstein's observations on voltage-dependent gating in colicin pore-forming toxins<sup>32,33</sup>, in which positively charged peptides flip across the membrane. The concept that voltage-sensor paddles carry gating charges across the membrane at the protein–lipid interface suggests many new experiments. In an accompanying paper, we pursue some of these ideas by examining the positions of the voltage-sensor paddles in the membrane, and determining how far the paddles move when the pore opens in response to membrane depolarization<sup>22</sup>. □

## Methods

### Channel expression and purification

KvAP was expressed and purified as described<sup>21</sup>. DNA for the isolated voltage sensor encoding Met 1 to Lys 147 was cloned into a pQE60 expression vector (Qiagen) between Ncol and BglII sites with a thrombin cleavage site followed by a C-terminal hexahistidine sequence. Protein was expressed in *E. coli* XL1-Blue cells by induction (at  $A_{600} \approx 1.0$ ) with 0.4 mM isopropyl-β-D-thiogalactopyranoside for 4 h at 37 °C. Cells were harvested and lysed in 50 mM Tris, pH 8.0, and 100 mM KCl, containing Leupeptin, Pepstatin, Aprotinin and phenylmethylsulphonyl fluoride (Sigma) to inhibit proteases. Protein was then extracted from the cell lysate for 3 h at room temperature in the above solution by adding 40 mM decylmaltose (DM), purified on a Talon Co<sup>2+</sup> affinity column (Clontech), and eluted with 5 mM DM, 20 mM Tris, pH 8.0, 100 mM KCl and 300–400 mM imidazole. Protein was incubated overnight at room temperature (~21 °C) in the presence of 1 unit of thrombin per 2 mg of protein to cleave the hexahistidine tag, and then further purified on a Superdex-200 (10/30) column (Pharmacia) in a solution of 30 mM n-octyl-β-D-glucoside (β-OG), 20 mM Tris, pH 8.0, and 100 mM KCl. For both KvAP and the isolated voltage sensor, analysis by MALDI-TOF mass spectrometry (Voyager-STR; PerSeptive Biosystems) and N-terminal sequencing indicated that the N terminus undergoes modification during expression in which the first five residues of the encoded constructs are replaced with a single leucine residue. Site-directed mutagenesis using QuickChange

(Stratagene) was used to generate more than 30 cysteine mutants of KvAP for derivatization with mercuric compounds. In each of the mutants, single residues within the S1–S5 region were replaced by cysteine. Purification was the same as for the wild-type channel. Five sites (V43C, A71C, A84C, R126C, L162C) gave useful difference electron density to assist model building.

### Toxin biochemistry

Isolated voltage sensor was expressed and purified as above, but without thrombin cleavage. Purified protein was applied to a 0.1 ml Co<sup>2+</sup> column to saturate the resin. Venom from *Grammostola spatulata* (SpiderPharm) was diluted tenfold in 20 mM Tris, pH 8.0, 100 mM KCl and 10 mM DM, and applied (0.1 ml) to the column saturated with isolated voltage sensor and to a control column with resin alone. Both columns were washed extensively to minimize nonspecifically bound toxins, first in the above buffer, then in the above buffer with 15 mM imidazole. Remaining protein was eluted from both columns with 0.1 ml of 400 mM imidazole, and reduced with 50 mM dithiothreitol at 37 °C for 2 h to improve separation by reverse-phase high-performance liquid chromatography (HPLC). Equal volumes of eluted, reduced protein from the two columns were run on an Agilent 1100 Series HPLC with a C-18 reverse-phase 5-μm, 80-Å column using a 2 min isocratic flow of 75% solution A (H<sub>2</sub>O, 0.1% trifluoroacetic acid, TFA) and 25% solution B (90% acetonitrile, 10% H<sub>2</sub>O, 0.1% TFA) followed by a 25–55% B gradient over 40 min. Peaks were collected and analysed by MALDI-TOF mass spectrometry. The peak corresponding to VSTX1 has the same retention time as purified, reduced VSTX1 run on the same gradient.

### Fab complex preparation

Monoclonal antibodies (mouse immunoglobulin) against KvAP were raised using standard procedures<sup>34</sup>. ELISA and western blot analysis were used to identify positive clones. Antibodies that recognized both KvAP and the isolated voltage sensor were selected. IgGs from mouse hybridoma cell culture supernatant were purified using a Protein A column (Bio-Rad). Fab fragments were generated by papain proteolysis (Worthington) and purified by Q-Sepharose chromatography. The sequences of the DNA encoding the variable region of Fabs were obtained as described<sup>24</sup>. KvAP (in DM) and the isolated voltage sensor (in β-OG) were mixed with Fabs (6E1 and 33H1, respectively) and concentrated. The complexes were purified on a Superdex-200 (10/30) column in a solution of 30 mM β-OG, 20 mM Tris, pH 8.0, and 100 mM KCl. The purified complexes were concentrated to about 10 mg ml<sup>-1</sup> using a 50-kDa molecular-mass cutoff Centriflon (Amicon) for crystallization.

### Crystallization

Crystals were grown by sitting-drop vapour diffusion at 20 °C by mixing equal volumes of protein and reservoir solutions. Fab 6E1-KvAP complex crystals were grown over a reservoir solution of 16–20% polyethylene glycol 400 (PEG400) or polyethylene glycol 350 monoethyl ether (PEGMME350), 150–200 mM CdCl<sub>2</sub> and 100 mM sodium acetate, pH 5.0. Crystals were of space group I422, with cell dimensions  $a = b = 189.4 \text{ \AA}$ ,  $c = 150.5 \text{ \AA}$ ,  $\alpha = \beta = \gamma = 90^\circ$ , and contained one KvAP subunit and one Fab in the asymmetric unit. Cryoprotection was achieved by raising the concentration of PEG400 or PEGMME350 in the reservoir to about 40%, after which crystals were frozen in liquid propane. Fab 33H1-isolated voltage-sensor complex crystals were grown over a reservoir solution of 20% PEG4000, 50 mM HEPES, pH 7.5. Crystals were of space group C2, with cell dimensions  $a = 264.7 \text{ \AA}$ ,  $b = 61.6 \text{ \AA}$ ,  $c = 46.1 \text{ \AA}$ ,  $\alpha = \gamma = 90^\circ$ ,  $\beta = 90.35^\circ$ , and contained one voltage sensor and one Fab in an asymmetric unit. Crystals were gently moved through paratone-N oil to remove excess solution surrounding the crystal, and were flash frozen under a cold nitrogen stream (~180 °C).

### Structure determination

All data were collected at ~180 °C under a nitrogen stream. For the Fab 6E1-KvAP complex crystals, multiple data sets (including those of cysteine mutants soaked in mercuric solution) were collected at Cornell High Energy Synchrotron Source (CHESS) A1 and F1, and National Synchrotron Light Source (NSLS) X25 beam lines. A crystal with a KvAP mutant (Tyr 46 being replaced by Cys) gave the best diffraction (3.2 Å). Data from Fab 33H1-isolated voltage-sensor domain crystals were collected at the CHESS A1 beam line. All data were indexed and integrated using DENZO and SCALEPACK<sup>35</sup>, and processed with CCP4 programs<sup>36</sup>. The Fab 6E1-KvAP structure was determined by molecular replacement using the program AMoRe<sup>37</sup> in CCP4 using a published Fab structure<sup>38</sup> (Protein Data Bank code 1BAF) as the search model. Because of the flexible connection between the Fab variable region (Fv) and constant region (Fc), these two units were used separately in the rotation and translation searches. After rigid-body refinement of the Fab fragment, a calculated electron density map using the phases from the Fab gave continuous electron density in the KvAP channel region. The cysteine mutants failed to provide useful phasing information owing to non-isomorphism; however, five sites (above) provided difference electron density maps to assist model building. The structure of the Fab 33H1-isolated voltage sensor was also determined by molecular replacement as described above. The complete models for both structures were built using O<sup>39</sup> and refined with CNS (Crystallography & NMR System)<sup>40</sup> by iterative cycles of simulated annealing and model rebuilding. The Fab 6E1-KvAP structure was refined against data to 3.2 Å to crystallographic and free residuals of 25.6% and 29.9% (using 5% of reflections), respectively. The final KvAP model contained residues 18–240. The N-terminal 17 residues and C-terminal 42 residues were disordered. Based on the presence of CdCl<sub>2</sub> and KCl in the crystallization solutions, seven Cd<sup>2+</sup> and six K<sup>+</sup> were modelled in the refined structure. The Fab 33H1-isolated voltage-sensor structure was refined against data to 1.9 Å with crystallographic and free residuals of 23.1% and 25.1% (using 5% of reflections), respectively. The first 19 residues of the isolated voltage sensor were disordered.

## Electrophysiology

KvAP channels were reconstituted from DM into lipid vesicles as described<sup>41</sup>, to give a final protein concentration of 200 µg ml<sup>-1</sup>. Planar lipid bilayers of 1-palmitoyl-2-oleoyl phosphatidylethanolamine (POPE; 15 mg ml<sup>-1</sup>) and 1-palmitoyl-2-oleoyl phosphatidylglycerol (POPG; 5 mg ml<sup>-1</sup>) in decane were painted over a 300 µm hole in a polystyrene partition separating the internal and external solutions. To induce fusion of channel-containing vesicles, solution on the side to which vesicles were added (*cis*) contained 150 mM KCl, 10 mM HEPES, pH 7.0, and the opposite side (*trans*) contained 15 mM KCl, 10 mM HEPES, pH 7.0. After the appearance of channels in the membrane, ion concentration on the *trans* side was increased to 150 mM KCl. VSTX1 was purified as described<sup>21</sup>.

Received 19 February; accepted 11 March 2003; doi:10.1038/nature01580.

1. Hille, B. *Ion Channels of Excitable Membranes* (Sinauer, Sunderland, Massachusetts, 2001).
2. Hodgkin, A. L. & Huxley, A. F. A quantitative description of membrane current and its application to conduction and excitation in nerve. *J. Physiol. (Lond.)* **117**, 500–544 (1952).
3. Armstrong, C. M. & Bezanilla, F. Charge movement associated with the opening and closing of the activation gates of the Na<sup>+</sup> channels. *J. Gen. Physiol.* **63**, 533–552 (1974).
4. Sigworth, F. J. Voltage gating of ion channels. *Q. Rev. Biophys.* **27**, 1–40 (1994).
5. Bezanilla, F. The voltage sensor in voltage-dependent ion channels. *Physiol. Rev.* **80**, 555–592 (2000).
6. Schoppa, N. E., McCormack, K., Tanouye, M. A. & Sigworth, F. J. The size of gating charge in wild-type and mutant Shaker potassium channels. *Science* **255**, 1712–1715 (1992).
7. Seoh, S. A., Sigg, D., Papazian, D. M. & Bezanilla, F. Voltage-sensing residues in the S2 and S4 segments of the Shaker K<sup>+</sup> channel. *Neuron* **16**, 1159–1167 (1996).
8. Aggarwal, S. K. & MacKinnon, R. Contribution of the S4 segment to gating charge in the Shaker K<sup>+</sup> channel. *Neuron* **16**, 1169–1177 (1996).
9. Noda, M. *et al.* Primary structure of *Electrophorus electricus* sodium channel deduced from cDNA sequence. *Nature* **312**, 121–127 (1984).
10. Tanabe, T. *et al.* Primary structure of the receptor for calcium channel blockers from skeletal muscle. *Nature* **328**, 313–318 (1987).
11. Tempel, B. L., Papazian, D. M., Schwarz, T. L., Jan, L. Y. & Jan, Y. N. Sequence of a probable potassium channel component encoded at the *Shaker* locus of *Drosophila*. *Science* **237**, 770–775 (1987).
12. Yang, N. & Horn, R. Evidence for voltage-dependent S4 movement in sodium channels. *Neuron* **15**, 213–218 (1995).
13. Larsson, H. P., Baker, O. S., Dhillon, D. S. & Isacoff, E. Y. Transmembrane movement of the Shaker K<sup>+</sup> channel S4. *Neuron* **16**, 387–397 (1996).
14. Yusaf, S. P., Wray, D. & Sivaprasadarao, A. Measurement of the movement of the S4 segment during the activation of a voltage-gated potassium channel. *Pflügers Arch.* **433**, 91–97 (1996).
15. Baker, O. S., Larsson, H. P., Mannuzzu, L. M. & Isacoff, E. Y. Three transmembrane conformations and sequence-dependent displacement of the S4 domain in Shaker K<sup>+</sup> channel gating. *Neuron* **20**, 1283–1294 (1998).
16. Mannuzzu, L. M., Moronne, M. M. & Isacoff, E. Y. Direct physical measure of conformational rearrangement underlying potassium channel gating. *Science* **271**, 213–216 (1996).
17. Cha, A. & Bezanilla, F. Characterizing voltage-dependent conformational changes in the Shaker K<sup>+</sup> channel with fluorescence. *Neuron* **19**, 1127–1140 (1997).
18. Horn, R. Coupled movements in voltage-gated ion channels. *J. Gen. Physiol.* **120**, 449–453 (2002).
19. Gandhi, C. S. & Isacoff, E. Y. Molecular models of voltage sensing. *J. Gen. Physiol.* **120**, 455–463 (2002).
20. Bezanilla, F. Voltage sensor movements. *J. Gen. Physiol.* **120**, 465–473 (2002).
21. Ruta, V., Jiang, Y., Lee, A., Chen, J. & MacKinnon, R. Functional analysis of an archaeabacterial voltage-dependent K<sup>+</sup> channel. *Nature* **422**, 180–185; advance online publication, 2 March 2003 (doi:10.1038/nature01473).
22. Jiang, Y., Ruta, V., Chen, J., Lee, A. & MacKinnon, R. The principle of gating charge movement in a voltage-dependent K<sup>+</sup> channel. *Nature* **423**, 42–48 (2003).
23. Doyle, D. A. *et al.* The structure of the potassium channel: molecular basis of K<sup>+</sup> conduction and selectivity. *Science* **280**, 69–77 (1998).
24. Zhou, Y., Morais-Cabral, J. H., Kaufman, A. & MacKinnon, R. Chemistry of ion coordination and hydration revealed by a K<sup>+</sup> channel–Fab complex at 2.0 Å resolution. *Nature* **414**, 43–48 (2001).
25. Jiang, Y. *et al.* Crystal structure and mechanism of a calcium-gated potassium channel. *Nature* **417**, 515–522 (2002).
26. Jiang, Y. *et al.* The open pore conformation of potassium channels. *Nature* **417**, 523–526 (2002).
27. Swartz, K. J. & MacKinnon, R. Mapping the receptor site for hanatoxin, a gating modifier of voltage-dependent K<sup>+</sup> channels. *Neuron* **18**, 675–682 (1997).
28. Swartz, K. J. & MacKinnon, R. Hanatoxin modifies the gating of a voltage-dependent K<sup>+</sup> channel through multiple binding sites. *Neuron* **18**, 665–673 (1997).
29. Lu, Z., Klem, A. M. & Ramu, Y. Ion conduction pore is conserved among potassium channels. *Nature* **413**, 809–813 (2001).
30. Santacruz-Toloza, L., Huang, Y., John, S. A. & Papazian, D. M. Glycosylation of Shaker potassium channel protein in insect cell culture and in *Xenopus* oocytes. *Biochemistry* **33**, 5607–5613 (1994).
31. Blaustein, R. O., Cole, P. A., Williams, C. & Miller, C. Tethered blockers as molecular ‘tape measures’ for a voltage-gated K<sup>+</sup> channel. *Nature Struct. Biol.* **7**, 309–311 (2000).
32. Slatin, S. L., Qiu, X. Q., Jakes, K. S. & Finkelstein, A. Identification of a translocated protein segment in a voltage-dependent channel. *Nature* **371**, 158–161 (1994).
33. Qiu, X. Q., Jakes, K. S., Kienker, P. K., Finkelstein, A. & Slatin, S. L. Major transmembrane movement associated with colicin Ia channel gating. *J. Gen. Physiol.* **107**, 313–328 (1996).
34. Harlow, E. & Lane, D. *Antibodies: A Laboratory Manual* (Cold Spring Harbor Laboratory Press, Cold Spring Harbor, 1989).
35. Otwinski, Z. & Minor, W. Processing of X-ray diffraction data collected in oscillation mode. *Methods Enzymol.* **276**, 307–326 (1997).
36. Collaborative Computational Project, N.4 The CCP4 suite: programs for X-ray crystallography. *Acta Crystallogr. D* **50**, 760–763 (1994).
37. Navaza, J. AMoRe: an automated package for molecular replacement. *Acta Crystallogr. A* **50**, 157–163 (1994).
38. Brunger, A. T., Leahy, D. J., Hynes, T. R. & Fox, R. O. 2.9 Å resolution structure of an anti-dinitrophenyl-spin-label monoclonal antibody Fab fragment with bound hapten. *J. Mol. Biol.* **221**, 239–256 (1991).
39. Jones, T. A., Zou, J. Y., Cowan, S. W. & Kjeldgaard, M. Improved methods for building protein models in electron density maps and the location of errors in these models. *Acta Crystallogr. A* **47**, 110–119 (1991).
40. Brunger, A. T. *et al.* Crystallography & NMR System: a new software suite for macromolecular structure determination. *Acta Crystallogr. D* **54**, 905–921 (1998).
41. Hegnbootham, L., LeMasurier, M., Kolmakova-Partensky, L. & Miller, C. Single *Streptomyces lividans* K<sup>+</sup> channels: Functional asymmetries and sidedness of proton activation. *J. Gen. Physiol.* **114**, 551–560 (1999).
42. Carson, M. Ribbons. *Methods Enzymol.* **277**, 493–505 (1997).
43. Thompson, J. D., Higgins, D. G. & Gibson, T. J. CLUSTAL W: improving the sensitivity of progressive multiple sequence alignment through sequence weighting, positions-specific gap penalties and weight matrix choice. *Nucleic Acids Res.* **22**, 4673–4680 (1994).

**Acknowledgements** We thank members of the MacKinnon laboratory for assistance at many stages of this project over five years. M. Long for biochemistry at early stages, J. Lee for studies of Ba<sup>2+</sup> on cell growth, D. Wang for teaching us to use the electron microscope, F. Weis-Garcia for assistance with monoclonal antibodies, the staff at CHESS A1 and F1 and NSLSX25, O. Andersen and D. Gadsby for manuscript critique, and R. Mohan for graphic work. This work was supported in part by a National Institutes of Health (NIH) grant to R.M., and by the National Center for Research Resources, NIH to B.T.C. V.R. is supported by a National Science Foundation Graduate Student Research Fellowship, and R.M. is an Investigator in the Howard Hughes Medical Institute.

**Competing interests statement** The authors declare that they have no competing financial interests.

**Correspondence** and requests for materials should be addressed to R.M. (mackinn@rockvax.rockefeller.edu). Coordinates have been deposited in the Protein Data Bank under accession codes 1ORQ and 1ORS.